




CASE REPORT OPEN ACCESS

Small Animal Internal Medicine Oncology

Multimodal Treatment of a Peripheral Primitive Neuroectodermal Tumor Originating From the Thoracic Cavity in a Dog

Leah H. Ackerman¹  | Madison Toonder¹ | Sarah Bosch¹ | Varvara B. Semenova¹ | Timothy P. Spicer² | Oscar Alas¹  | Lily S. Thorsen¹ | Aitor Gallestegui Menoyo¹ | Valentina B. Stevenson¹ | Jishnu Rao Gutti¹ | Paulo Vilar Saavedra¹ | Rebecca Nance¹ | Bakash Sahay³ | Gabriela P. Hery¹ | Ann M. Chan¹ | Marc E. Salute¹ | Nesrine Bensilmane² | Virneliz Fernandez Vega² | Rowan J. Milner¹ 

¹Department of Small Animal Clinical Sciences, University of Florida College of Veterinary Medicine, Gainesville, Florida, USA | ²Department of Molecular Medicine, The Herbert Wertheim University of Florida Scripps Institute, Jupiter, Florida, USA | ³Department of Infectious Diseases & Immunology, University of Florida College of Veterinary Medicine, Gainesville, Florida, USA

Correspondence: Leah H. Ackerman (leahackerman95@ufl.edu)

Received: 9 October 2024 | **Revised:** 18 February 2025 | **Accepted:** 24 February 2025

Funding: This work was supported by the Milner Comparative Oncology Lab.

Keywords: Askin's tumor | cancer | chemotherapy | dog | precision medicine | primordial neoplasia

ABSTRACT

Peripheral primitive neuroectodermal tumor (pPNET) is a very rare, highly malignant tumor encountered in young dogs, with only four necropsy cases in the veterinary literature. A 1.5-year-old male intact French Bulldog presented for evaluation of progressive left forelimb lameness and ipsilateral Horner's syndrome. Whole body computed tomography identified a 12 cm mediastinal mass with extension into the vertebral canal and multifocal metastatic lesions. Histological and immunohistochemical results were consistent with a pPNET. Chemotherapy, radiation therapy, immunotherapy, and targeted therapy were administered. Precision-based tumor testing, including DNA sequencing and chemosensitivity assays, were performed to guide systemic treatment recommendations. A partial remission was observed 3.5 months from presentation based on imaging and improved clinical status. After 7 months of treatment, diffuse metastatic disease, including intracranial spread, was observed and the dog was euthanized.

1 | Introduction

Primitive neuroectodermal tumor (PNET) is a rare, highly metastatic tumor that originates from the embryonic neural tube. It affects adolescents across numerous species, including humans and dogs. This tumor is further subcategorized by location: central, neuroblastoma (autonomic), and peripheral (pPNET) [1–3]. In humans, pPNET has been found to arise from the abdominal cavity, retroperitoneal space, or thoracic cavity. In human

medical literature, pPNET poses a diagnostic challenge; it often is mistaken for other neoplasms with a round cell appearance, including lymphoma and rhabdoid tumors. These tumors require a histologic diagnosis using immunoreactivity for glial or neural markers [2, 4, 5].

Given its scarcity, pPNET is not well characterized in the veterinary medical literature. Currently, more data is available on central PNET across species [2, 4, 6, 7]. In human adolescents, even

Abbreviations: 3D, three dimensional; ATP-TCA, ATP-based chemosensitivity assay; CHOP, multi-agent weekly chemotherapy protocol consisting of cyclophosphamide, hydroxydaunorubicin, oncovin, and prednisone; cKIT, tyrosine-proteinase KIT; CT, computed tomography; EC50, lowest half maximal effective concentration response; FC, flow cytometry; FNA, fine needle aspirate; GFAP, glial fibrillary acidic protein; IHC, immunohistochemistry; MRI, magnetic resonance imaging; NCI, National Cancer Institute; PARR, PCR for antigen receptor rearrangements; PCR, polymerase chain reaction; pPNET, peripheral primitive neuroectodermal tumor; UFSAH, University of Florida's Small Animal Hospital.

This is an open access article under the terms of the [Creative Commons Attribution-NonCommercial-NoDerivs](https://creativecommons.org/licenses/by-nc-nd/4.0/) License, which permits use and distribution in any medium, provided the original work is properly cited, the use is non-commercial and no modifications or adaptations are made.

© 2025 The Author(s). *Journal of Veterinary Internal Medicine* published by Wiley Periodicals LLC on behalf of American College of Veterinary Internal Medicine.

with multimodal local and systemic therapy, the median survival time for patients with pPNET ranges from 15 to 23 months [4, 7]. Only four cases of pPNET in dogs are represented in published necropsy case reports, none of which included multimodal precision-based treatment and response data [2, 6, 8, 9].

2 | Case Description

A 1.5-year-old 9 kg male intact French Bulldog presented to the University of Florida's Small Animal Hospital (UFSAH) for a 4-month history of progressive left forelimb lameness and a 12-month history of ipsilateral Horner's syndrome.

On presentation, the dog was quiet, alert, and responsive with adequate hydration, normal mentation, normal capillary refill time, and pink mucosal membranes. Heart rate was 95 beats per minute, respiratory rate 36 breaths per minute, and temperature 100.9°F. Left ocular miosis and ptosis were observed. The dog had bilaterally stenotic nares, moderate stertor, muffled lung sounds, left-sided hemiparesis with delayed proprioceptive deficits, cranial thoracic spinal pain, and absent left-sided panniculus reflex.

Initial diagnostics tests included a CBC, serum biochemistry panel, thoracic radiographs, abdominal ultrasound examination, and fine needle aspirates (FNA). No clinically relevant findings were observed on laboratory tests. Thoracic radiographs indicated cranial mediastinal widening with partial effacement of the cranial borders of the cardiac silhouette, left cranial lung lobe atelectasis and displacement, and tracheal deviation to the right side. Abdominal ultrasound examination identified a 2.9×1.8×1.7 cm well-defined heterogeneously hyperechoic abdominal mass located cranial to the left kidney and lateral to the adrenal gland. Cytologic evaluation of ultrasound-guided FNAs of the mediastinal mass and cranial abdominal mass was consistent with large cell lymphoma (Figure 1). A multi-agent cyclophosphamide, hydroxydaunorubicin, vincristine, and prednisone chemotherapy protocol (CHOP) was initiated, and the patient received vincristine (0.6 mg/m² IV) and a tapering course of prednisone (starting at 2 mg/kg q 24h over 4 weeks). Additional FNA samples of the mediastinal mass and cranial abdominal mass were collected for flow cytometry (FC) and PCR for antigen receptor rearrangements (PARR).

Flow cytometry identified 39% cell viability, including mixed inflammatory cells (small lymphocytes, neutrophils, monocytes) and a population of large cells that did not express CD45, CD21, CD3, CD4, or CD8, among other leukocyte markers. The patient received two doses of vincristine and one dose of cyclophosphamide (227 mg/m² PO), while awaiting PARR results, with progressive tachypnea and dyspnea and no appreciable improvement in lameness. The PARR results indicated a polyclonal lymphoid population, suggesting that the large cell population previously observed on FC was not of lymphoid origin.

The dog underwent magnetic resonance imaging (MRI) of the cervical and cranial thoracic vertebral column, 1 month after initial presentation (Figure 2). Multiplanar pre- and post-IV contrast sequences were acquired using a 1.5 Tesla magnet (Toshiba Titan, Canon Medical Systems Inc., USA, 2441 Michelle Drive

Tustin, CA, 92780). A well-defined, rounded, T2 hyperintense, moderately homogeneous contrast-enhancing nodule occupied up to 80% of the left ventrolateral aspect of the spinal cord at the level of T2. In the cranial mediastinum, a large, heterogeneously mild-to-moderate T2 hyperintense and heterogeneously contrast-enhancing mass extended into the vertebral canal at T1–2.

Computed tomography (CT) was performed (Figure 3) using an Aquilion Prime 160 multi-detector helical CT scanner (Canon Medical Systems Inc. USA, 2441 Michelle Drive Tustin, CA 92780) at 120 kVp and 300 mA, using a soft tissue and bone algorithm with radiation planning utilizing a vacuum-lock bag. This study identified a well-defined, smoothly margined, mixed-fluid-to-soft tissue attenuating 3 cm mass abutting the lateral aspect of the left adrenal gland, in addition to the findings observed on MRI.

Multiple FNAs and ultrasound-guided Tru-Cut (Merit Medical, UT, 1987) 14 g biopsy samples were acquired from the cranial mediastinal mass and left cranial abdominal mass. The excised biopsy samples were immersed in 10% buffered formalin and submitted for histopathology and immunohistochemistry (IHC). Histologically, the neoplasm was multilobulated and composed of a small, polygonal cell population arranged in dense packets, nests, and sheets on a fine fibrovascular stroma (Figure 4A). The neoplastic cells frequently palisaded along vascular adventitia and occasionally formed radial arrangements surrounding eosinophilic fibrillar material (Homer-Wright rosettes; Figure 4B). The cells had indistinct cell borders, some eosinophilic homogeneous cytoplasm, and oval, hyperchromatic nuclei with variably distinct, central nucleoli. Mitotic figures were 14 in 2.37 mm². Anisocytosis and anisokaryosis were moderate. Approximately 20% of neoplastic cells exhibited moderate, multifocal, granular cytoplasmic immunoreactivity with tyrosine proteinase KIT (cKIT) IHC (Figure 4C). Neoplastic cells exhibited marked membranous and moderate cytoplasmic immunoreactivity for synaptophysin (Figure 4D) and negative immunoreactivity for glial fibrillary acidic protein (GFAP) on IHC.

Flow cytometry from FNA samples of the cranial abdominal mass indicated dual cell surface expression of gangliosides GD3 and GD2 (Figure S1).

Remaining tissue samples were submitted for DNA sequencing (SearchLight DNA, Vidium Animal Health, 7201 E Henkel Way, Suite 210, Scottsdale, AZ 85255), which identified 12 copy number loss mutations (*ATM*, *ERRF1*, *FANCA*, *FANCL*, *FLCN*, *KMT2D*, *MSH2*, *MSH3*, *PALB2*, *PMS2*, *TP53*, and *TSC2*) and 4 therapeutic recommendations based on observed mutations (Everolimus, Olaparib, Carboplatin, and Sirolimus).

The dog received doxorubicin (1 mg/kg IV) the day after CT. Palliative radiation (Varian Edge Linear Accelerator, Varian Medical Systems Inc., 3100 Hansen Way, Palo Alto, CA 94304) was administered, consisting of 4 Gy daily for 5 consecutive days (6 megavoltage), 6 days after doxorubicin administration (Figure S2).

A marked clinical response was observed 1 week after radiation treatment, at which time the dog received its first immunotherapy

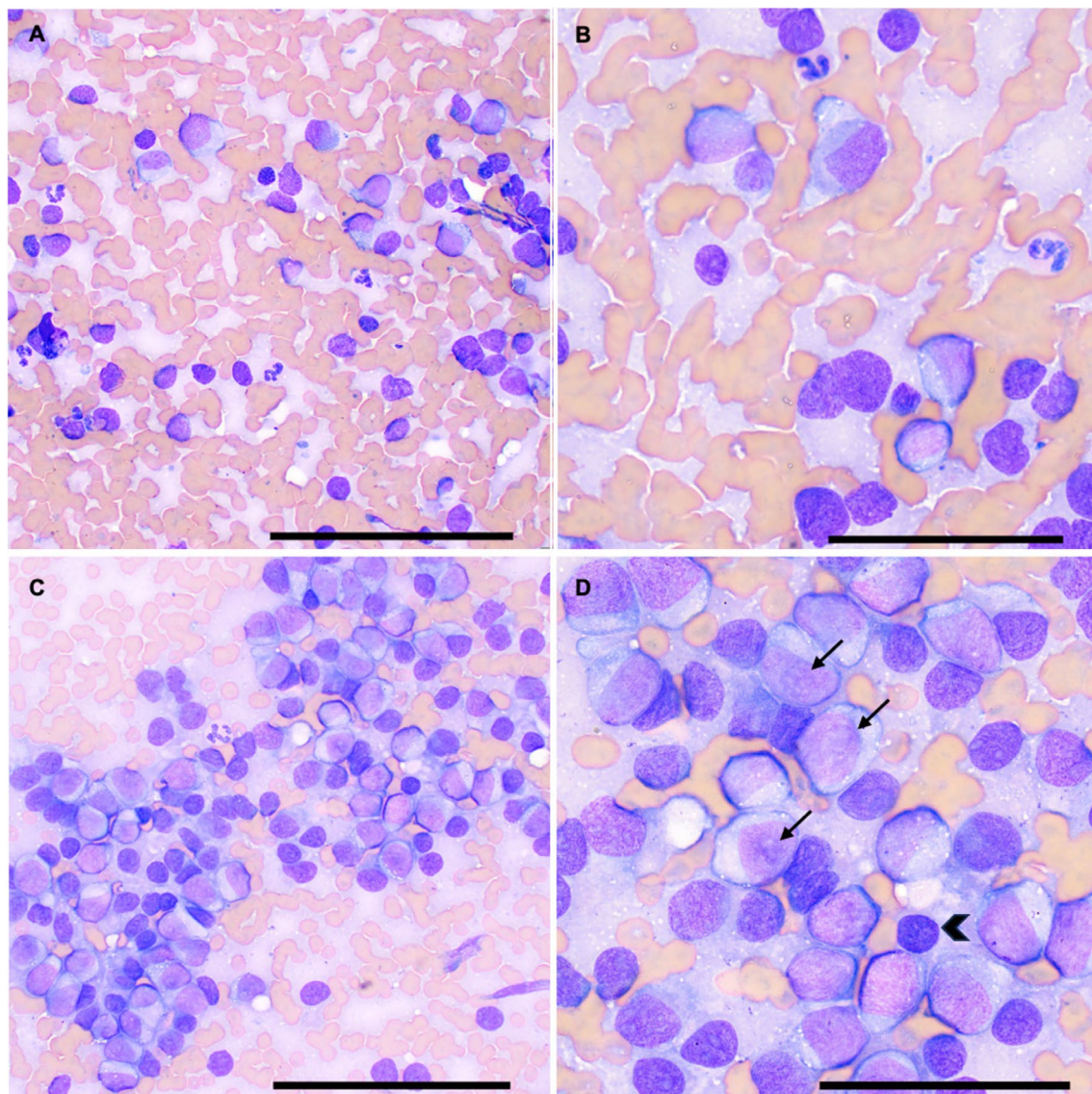


FIGURE 1 | Fine needle aspirate biopsy of a cranial abdominal mass (A, B) and a mediastinal mass (C, D) from a 1.5-year-old male French Bulldog. Wright-Giemsa stain. (A) The sample from the cranial abdominal mass was moderately cellular and contained many lysed cells and free nuclei. When intact, large, discrete round cells, initially classified as lymphocytes, were arranged individually or in small, poorly cohesive to non-cohesive groupings. 50× oil immersion magnification. Scale bar = 100 μm. (B) Higher magnification of the large, discrete round cell population of the cranial abdominal mass. The intact round cells contain a small amount of light blue, often faintly vacuolated cytoplasm with eccentric nuclei which measured larger than the diameter of a neutrophil, with finely stippled chromatin and 0–2 faint nucleoli. 100× oil immersion magnification. Scale bar = 50 μm. (C) The sample from the mediastinal mass was more cellular and consisted of a similar population of large, discrete round cells identical to the cells appreciated in the cranial abdominal mass. 50× oil immersion magnification. Scale bar = 100 μm. (D) Higher magnification of the cranial mediastinal mass shows the nucleoli more clearly (black arrows). Few small lymphocytes were also observed (black arrowhead). A cytologic diagnosis of large cell lymphoma was made and flow cytometry was recommended for follow up. 100× oil immersion magnification. Scale bar = 50 μm.

consisting of a GD3/GD2 liposomal vaccine (UF CVM Clinical Trial, Gainesville, FL, USA) with alternating doxorubicin treatments every 3 weeks for a total of 6 cycles (doxorubicin day 1, 21; vaccine day 14). Restaging with thoracic radiographs and abdominal ultrasound examination at doxorubicin dose #4 indicated partial resolution of both the cranial abdominal mass, which measured 0.8 cm, and the cranial mediastinal mass.

At doxorubicin dose #6, physical examination identified new right prescapular lymphadenomegaly, measuring 2.5 cm. A recheck CT was performed to assess treatment response (Figure 5). The previously described mediastinal mass had

markedly decreased in size and no longer extended into the vertebral canal, with resolved spinal cord compression. Newly identified within the left caudal pleural space was a well-defined, ovoid, soft tissue-attenuating, contrast-enhancing nodule. The findings were compatible with an overall localized response to treatment, but FNA cytology of the pleural nodule and right prescapular lymph node was consistent with metastatic pPNET.

The patient then received carboplatin (10 mg/kg IV) and rapamycin (0.1 mg/kg q48h) based on SearchLight DNA results, 3 weeks later. Immunotherapy was continuously administered every 3 weeks. The dog was restaged using whole-body CT and

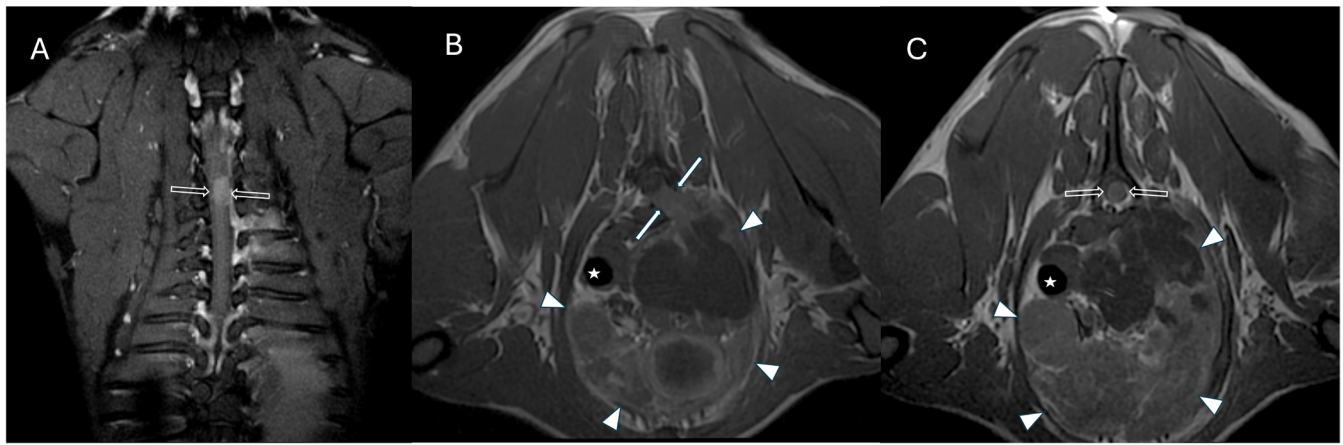


FIGURE 2 | Magnetic resonance imaging cranial thoracic vertebral column. (A) Dorsal T1W fat saturation; (B) T1W transverse post-gadolinium at T1-T2; (C) T1W transverse post-gadolinium at T2. Intramedullary nodule at the level of the second thoracic vertebra (A and C, white rim arrows). Large, multilobulated, contrast enhancing, cranial mediastinal mass (B and C, white arrowheads) that causes severe rightward displacement of the trachea (B and C, white star), and extension into the left intervertebral foramen with severe widening and into the ventral vertebral canal with severe compression and rightward deviation of the spinal cord (B, solid white arrows).



FIGURE 3 | Computed tomography cranial thorax. (A) pre-contrast transverse at T1-T2; (B) post-contrast transverse at T1-T2; (C) post-contrast dorsal; (D) post-contrast transverse at T2. (A and B) a large, multilobulated, soft tissue attenuating, contrast enhancing cranial mediastinal mass (white arrowheads) causes severe rightward displacement of the trachea (white star) and extension into the left intervertebral foramen with severe widening (solid white arrows) and extension into the ventral vertebral canal with severe compression and rightward deviation of the spinal cord. (C) large, multilobulated, soft tissue attenuating, contrast enhancing cranial mediastinal mass (white arrowheads), and rim enhancing fluid and soft tissue attenuating mass craniomedial to the left kidney (white rim arrow). (D) Intramedullary nodule at the level of the second thoracic vertebra (solid white arrow).

radiation planning 3 weeks after carboplatin administration to assess response to immunotherapy; CT identified a static mediastinal mass and new progressive multifocal pleural nodules (> 3.7 cm), cranial mediastinal lymphadenomegaly (1.7 cm), left sternal lymphadenomegaly (1.2 cm), right and left medial iliac lymphadenomegaly (1.2 and 1.6 cm respectively), and a left renal nodule (0.7 cm). Cytologic evaluation of FNAs of medial iliac lymph nodes and the left renal nodule was consistent with metastatic pPNET.

Additional right prescapular lymph node FNAs were obtained for the National Cancer Institute (NCI) approved oncology drug set (179 drugs). Cells were delivered to Herbert Wertheim UF Scripps Institute (Gainesville, FL, USA). Cells were dissociated using 0.05% trypsin and counted. Cells exhibited excellent viability of 99.6%. Five-hundred cells/well were plated in 5 μ Ls of culture medium (Dulbecco's Modified Eagle Medium + 10% Fetal Bovine

Serum+1% Anti-Anti) into 1536 cell repellent 3-dimensional (3D) plates (Part#789979, Greiner, Bio-One, NC, USA). This process allows cell aggregation into 3D primary spheroids, which more accurately mimics the native tumor environment [10, 11]. The 179 drugs obtained from the NCI were transferred as 10 nL volumes into the test wells containing the tumor cells in triplicate as 10-point 3-fold serial dilutions. These plates were incubated for 24 h at 37°C, in 5% CO₂, using a 45° angle plate adaptor to generate the spheroids [12]. After 72 h, the viability of the spheroids was determined by adding 5 μ L per well of Cell Titer-Glo 3D (Part # G96683, Promega, Madison, WI, USA). Luminescence was detected using the PHERAStar (BMG LABTECH, Ortenberg, Germany, 2024) plate reader. Raw data was exported into the UF Scripps database and normalized according to company protocol.

Among the 179 drugs tested, potentially useful drugs were identified based on the lowest half maximal effective concentration

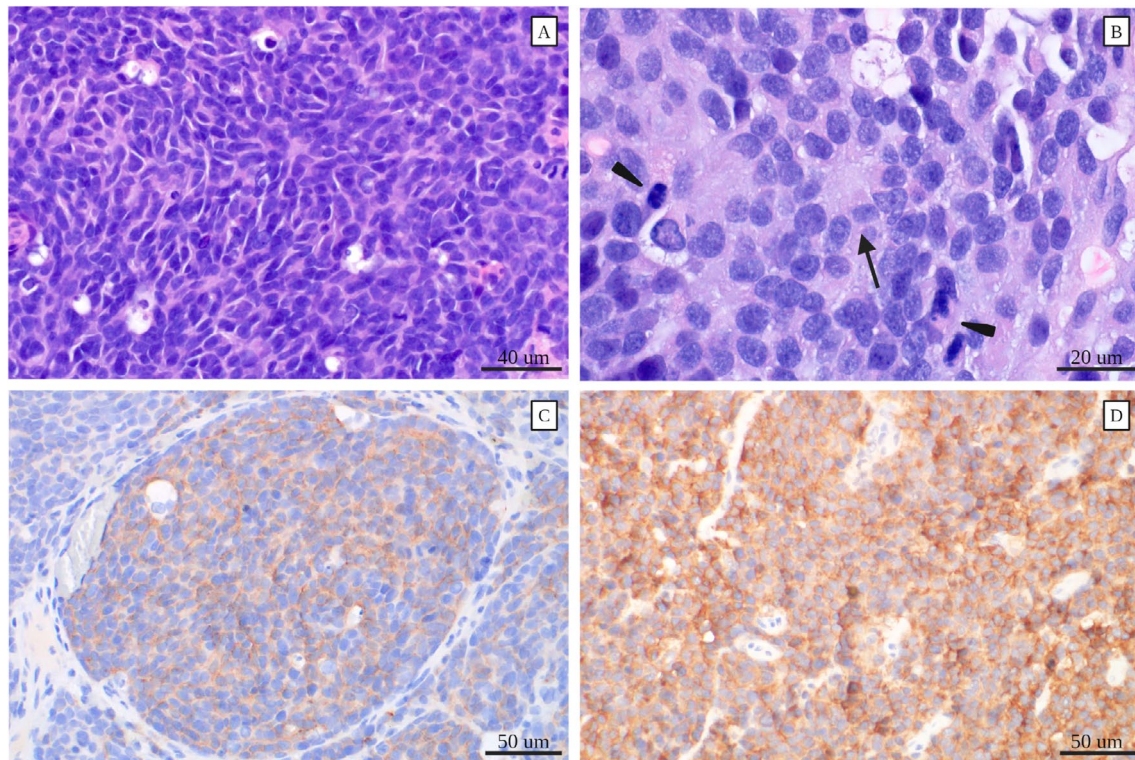


FIGURE 4 | Photomicrographs of the neoplasm. (A) Sheets and aggregates of polygonal to triangular neoplastic cells. (H&E, 500× magnification). (B) The cells multifocally form Homer-Wright rosettes (arrow) and have frequent mitotic activity (arrowheads). (H&E, 1000× magnification). (C) Some neoplastic cells exhibit moderate cytoplasmic staining with c-KIT IHC. (400× magnification). (D) All neoplastic cells exhibit cytoplasmic staining with synaptophysin IHC. (400× magnification).

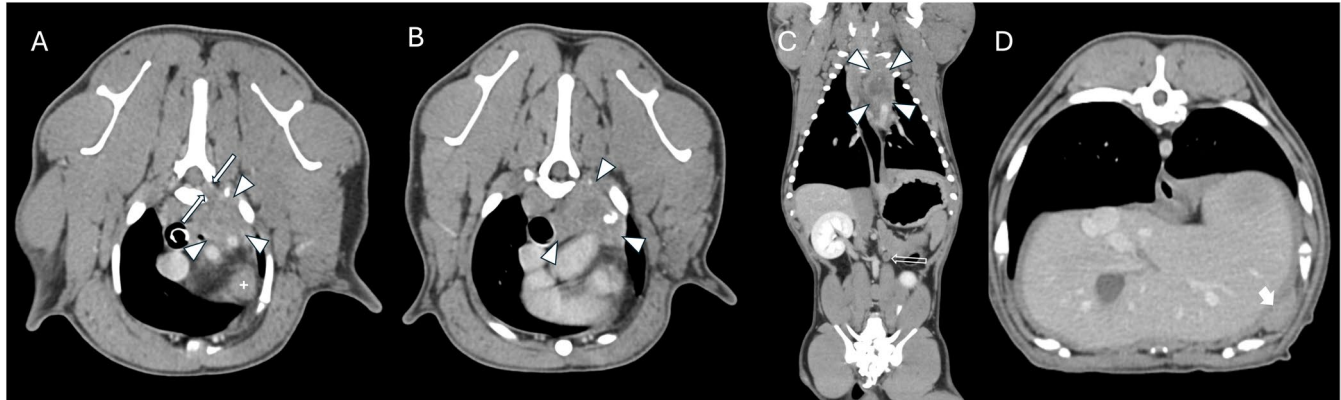


FIGURE 5 | Computed tomography (CT) of thorax and abdomen after radiotherapy and intravenous chemotherapy. (A) post-contrast transverse at the level of T1-T2; (B) post-contrast transverse at the level of T2; (C) dorsal reformatted post-contrast; (D) post-contrast transverse at the level of the diaphragm. (A) marked reduction in size of the cranial mediastinal mass (white arrowheads) with minimal extension into the left intervertebral foramen with similar widening (solid white arrows) and resolved extension into the left ventral vertebral canal. A cranial mediastinal lymph node is enlarged (white cross). (B) intramedullary lesion not identified at the level of T2 with marked reduction in size of the cranial mediastinal mass (white arrowheads). (C) marked reduction in size of the cranial mediastinal mass (white arrowheads) and left cranial abdominal mass (open white arrow). (D) newly identified left caudal pleural space soft tissue nodule (thick white arrow).

response (EC50) and the highest average maximum percentage response [12]. These drugs included romidepsin, carfilzomib, auranofin, methotrexate, belinostat, bortezomib, panobinostat, doxorubicin, and mitoxantrone.

One week after CT, the dog received a second palliative radiation treatment consisting of 4Gy×5 consecutive days to the

residual mediastinal disease and progressive multifocal metastases (Figures S3A and S3B).

The dog received methotrexate (0.75 mg/kg IV) 17 days after radiation. Methotrexate was combined with mitoxantrone (5 mg/m² IV) at methotrexate dose #2 (8 days from the previous dose), at which time the dog exhibited stranguria and pollakiuria. Mild

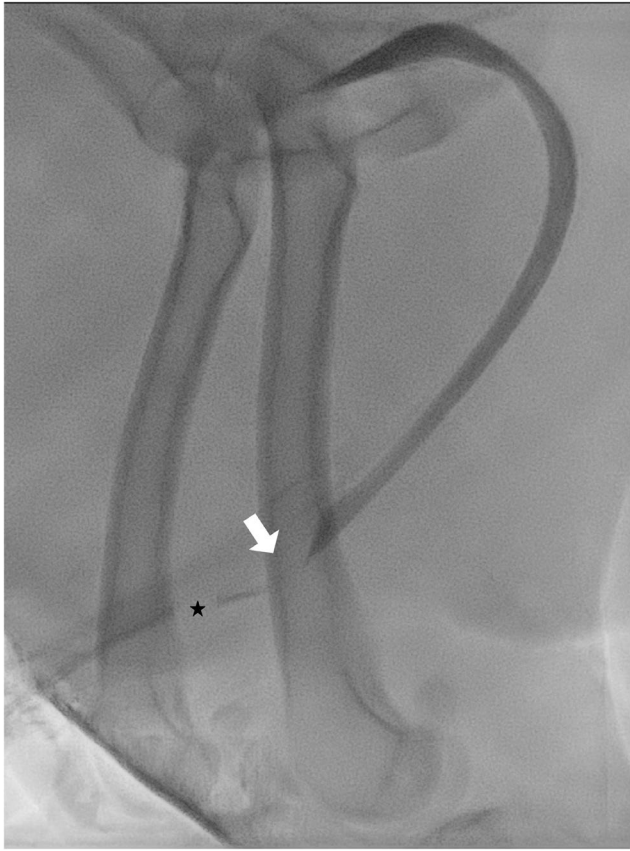


FIGURE 6 | Positive contrast retrograde urethrogram. Ventral to the mid-caudal aspect of the os penis, there is a broad-based dorsal filling defect of the urethra (white arrow). Cranial to this filling defect there is an additional, smaller, oval, and centrally located filling defect (black star) consistent with artifact from a transient gas bubble administered during the retrograde injection of positive contrast (Iohexol 350 mgI/ml at 1:1 dilution; GE HealthCare, 500 West Monroe Street, Chicago, Illinois, 60661).

right-sided temporalis muscle atrophy was noted on physical examination. Urinalysis disclosed marked pyuria and moderate bacteriuria with cocci and bacilli. The dog was started on amoxicillin/clavulanate and enrofloxacin.

Twenty-nine weeks after initial presentation, the dog presented with persistent stranguria and decreased urine output. A positive contrast retrograde urethrogram was obtained using an Azurion interventional fluoroscopic suite (Philips Healthcare, 3000 Minuteman Rd., Andover, MA 01810) and identified a penile urethral mass (Figure 6). Cytology of the penile urethral mass was consistent with metastatic pPNET.

Full staging then was performed using head MRI (Figure 7) acquired using a Vantage Orian 1.5T magnet (Canon Medical Systems Inc., USA, 2441 Michelle Drive Tustin, CA, 92780). Multifocal intracranial masses were identified, with involvement of the right facial, vestibulocochlear, and trigeminal nerves (Figure 7A,B) and secondary right-sided masticatory muscle atrophy, left dorsolateral transcalvarial extension (Figure 7D), and pituitary gland involvement (Figure 7C), respectively. The largest mass was associated with transfalxine herniation and increased intracranial pressure (Figure 7C,D). A concurrent full-body CT (Figure 8) verified lesions identified on the MRI. The mediastinal mass appeared markedly decreased in size (Figure 8A,B). Coalescing, soft tissue-attenuating, contrast-enhancing nodules were observed in the left caudo-dorsolateral pleural space, and resulted in extra-pleural signs (Figure 8C). The left kidney had two capsular deforming nodules and a small mass (Figure 8F). Newly identified small masses were noted along the left ventrolateral body wall (Figure 8D,E). Given the diffuse metastatic disease with subsequent urethral obstruction and intracranial involvement, euthanasia was elected 231 days after initial presentation and 596 days after initial presenting clinical signs.

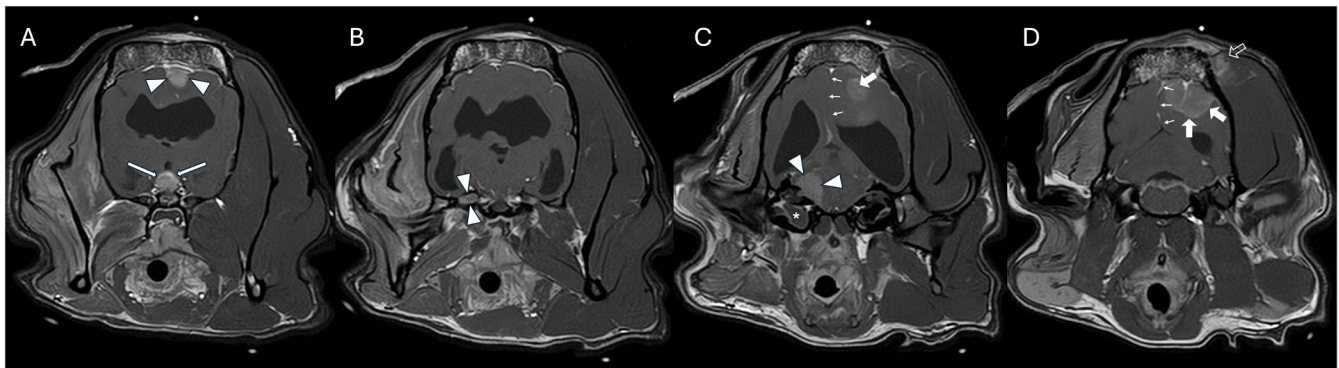


FIGURE 7 | Magnetic resonance imaging (MRI) of the head. Transverse plane and T1w post gadolinium images at the level of the pituitary gland (A), the trigeminal ganglion (B), the internal acoustic meatus (C); and the cerebellum (D). In the dorsal aspect of the brain and to the left of midline there is a fairly well-defined mass (A, white arrow heads) and centered on the pituitary gland there is a second smaller, rounded, well-defined mass (A, long white arrows). Centered at the level of the right acoustic meatus and the plane of the vestibular and facial nerves there is a third, broad-based and well-defined, contrast enhancing mass (C, white arrowheads). This mass extends rostrally along the path of the right trigeminal and results in widening of the right trigeminal ganglion (B, white arrowheads). Concurrently the right temporal, masseter, pterygoid, and digastricus muscles are small compared to the right and exhibit moderate contrast enhancement. The right tympanic bulla is fluid filled (C, white star) and the mucosa creates a rim contrast enhancement. At the left dorsal aspect of the cerebrum an additional, broad based, mildly lobular, well defined, and contrast enhancing mass (D and C, thick white arrows) causes rightward deviation of the longitudinal cerebral fissure (D and C, thin white arrows). This mass extends across the diploe of the calvarium into the dorsolateral soft tissues (D, thick white border arrow). Right side of the head is to the left of the image.

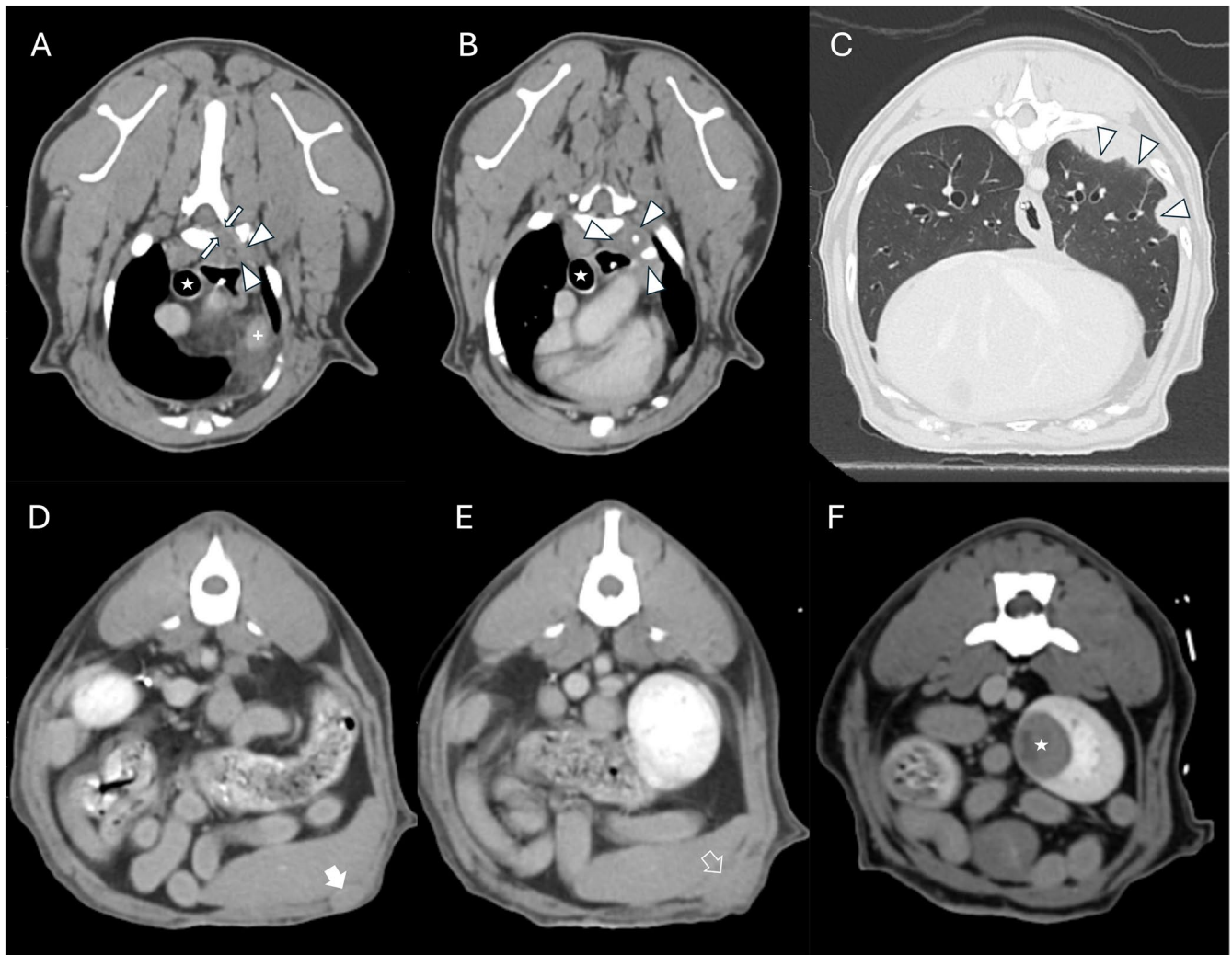


FIGURE 8 | Computed tomography (CT) of the thorax and abdomen. (A) post-contrast transverse soft tissue algorithm at T1-T2; (B) post-contrast transverse soft tissue algorithm at heart base; (C) transverse lung algorithm at T9-10; (D) post-contrast transverse soft tissue algorithm at L2; (E) post-contrast transverse soft tissue algorithm at L3; (F) post-contrast transverse soft tissue algorithm at cranial pole of left kidney. The previously described left dorsal mediastinal mass is markedly small (A and B, white arrowheads) with increased hyperattenuating foci of mineralization, and maintains extension through the T1-2 left intervertebral foramen (A, white long arrows), with resolved spinal cord compression and rightward displacement of the trachea (A and B, white star). A cranial mediastinal lymph node remains enlarged (A, white cross). In the left dorsolateral pleura, there are multiple, variably coalescing, fairly well defined, broad-based nodules and masses that cause multifocal extra-pleural signs (C, white arrowheads). In the left ventral abdominal body wall, there are a persistent small, well defined, oval, soft tissue nodule (D, thick white arrow) and a new small, lobular, soft tissue mass (E, thick white arrow rim). A heterogeneously contrast enhancing mass in the cranial pole of the right kidney (F).

3 | Discussion

Only four cases of pPNET have been reported in the veterinary literature. Previously reported dogs with this rare and primitive disease were euthanized because of poor prognosis [13].

In humans, pPNET arising from the thoracopulmonary region is referred to as Askin's tumor [2]. Patients with Askin's tumor present at an average age of 14 years with a painful thoracic wall mass, dyspnea, cough, weight loss, Horner's syndrome, regional lymphadenopathy, or some combination of these findings. The rare occurrence and atypical presentation of neoplasia in youth, and non-specific cytologic appearance, make pPNET a diagnostic challenge across species [2]. A definitive diagnosis requires histopathology and IHC with characteristic features including the presence of Homer-Wright

rosettes, CD99 IHC expression, and additional neural markers [14]. The tumor frequently is mistaken for other small, round cell tumors, such as embryonal rhabdomyosarcoma, neuroblastoma, or lymphoma in humans [4]. In dogs, lymphoma typically is a cytologic diagnosis and is the most common neoplasm diagnosed in young dogs [15]. The discrepancy between initial cytologic diagnosis and molecular results, in combination with a lack of response to a CHOP-based chemotherapy protocol in our case, ultimately led to further investigation with advanced imaging, biopsy, and IHC, resulting in the diagnosis of a pPNET based on the presence of an invasive intra-thoracic mass, Homer-Wright rosettes, positive synaptophysin staining, and positive ganglioside staining [7].

Because of the aggressive nature of pPNET in people, we employed a similar and aggressive multimodal treatment utilizing

radiation therapy, cytotoxic chemotherapy, targeted therapy, and immunotherapy [5, 16–18]. Reported treatment in people includes radical surgical resection, radiation (40–50 Gy average) and multi-agent chemotherapy including doxorubicin, actinomycin D, cyclophosphamide, ifosfamide, vincristine, etoposide, busulfan, melphalan, and carboplatin [17, 19]. The prognosis of Askin's tumor in children is poor, with a median survival time of 7–8 months with monotherapy and 15 months with multimodal treatment [17, 20].

The GD2 and GD3 glycosphingolipids are overexpressed in a wide variety of tumors in humans and thus serve as potential therapeutic targets [21]. Ganglioside GD3 is expressed across dogs and humans in neuroprogenitor cells, melanoma, and osteosarcoma, among other neoplasms [21]. Ganglioside GD3 expression in melanoma is associated with enhanced proliferation, adhesion, and invasive activity [21]. Upregulation of GD3 has been found in various neuroectodermal tumors of humans [22]. High expression of GD2 has been noted in neuroblastoma and Ewing sarcoma [16, 21, 22]. The observed expression of GD2 and GD3 in our dog's tumor not only supported our diagnosis but also served as a therapeutic target. The patient received 7 dual GD3/GD2 targeted liposomal vaccines throughout its treatment protocol.

An individualized or precision-based approach to cancer treatment is not common in veterinary oncology because of typical financial constraints. In our patient, this approach included DNA sequencing, flow cytometry to assess ganglioside expression, and tumor chemosensitivity testing using the NCI panel of 179 drugs and the ATP-based chemosensitivity assay (ATP-TCA) [5, 23]. This assay has been used in humans with lung cancer, ovarian cancer, cervical cancer, esophageal cancer, and breast cancer, exhibiting a beneficial relationship with clinical outcomes based on chemoresistance and sensitivity assessment [10, 11, 15, 24, 25]. The personalized combination of radiation therapy (40 Gy total), cytotoxic chemotherapy (doxorubicin, carboplatin, methotrexate, mitoxantrone, vincristine, cyclophosphamide), prednisone, targeted therapy (rapamycin), and immunotherapy (GD3/GD2 vaccine) resulted in a survival time of 20 months after the initial development of Horner's syndrome in our patient. Clinical progression was noted after vincristine and cyclophosphamide administration. The palliative radiation protocols, doxorubicin, and immunotherapy resulted in a partial response. Progressive disease was noted after carboplatin combined with rapamycin and methotrexate combined with mitoxantrone. This novel case describes the resolution of an exceptional diagnostic dilemma, a multimodal personalized-based oncologic treatment approach, and an outcome that exceeded preconceived prognostic expectations in a dog with a very rare, aggressive tumor. These results emphasize the potential of a personalized and multimodal oncologic approach for the treatment of pPNET, paving the way for future clinical trials and treatment options for affected dogs and serving as a model for further investigations and potential treatments for humans with pPNET.

Acknowledgments

Funding from the Milner Comparative Oncology Lab (University of Florida College of Veterinary Medicine) was provided for cell culture and GD3/GD2 flow cytometry.

Disclosure

Enrofloxacin and Augmentin (amoxicillin and clavulanate potassium) used off-label.

Ethics Statement

Authors declare no Institutional Animal Care and Use Committee or other approval was needed. Authors declare human ethics approval was not needed.

Conflicts of Interest

The authors declare no conflicts of interest.

References

1. D. Sturm, B. A. Orr, U. H. Toprak, et al., "New Brain Tumor Entities Emerge From Molecular Classification of CNS-PNETs," *Cell* 164, no. 5 (2016): 1060–1072, <https://doi.org/10.1016/j.cell.2016.01.015>.
2. A. Hespel, M. De Swarte, K. Anderson, R. Weiss, and J. Hathcock, "Features of a Rare Peripheral Primitive Neuroectodermal Tumour Arising From the Thoracic Spine in a Juvenile Canine Patient," *Veterinary Medicine and Science* 7, no. 3 (2021): 680–685, <https://doi.org/10.1002/vms3.449>.
3. D. J. Meuten, ed., *Tumors in Domestic Animals*, Fifth ed. (Ames, Iowa, 2017).
4. J. Peng and X. M. Han, "The Prognostic Factors of Ewing Sarcoma/Peripheral Primitive Neuroectodermal Tumor: A Retrospective Analysis of 67 Patients at a Single Center," *Medicine* 101, no. 29 (2022): e29564.
5. K. Katayama, K. Kuroki, K. Uchida, et al., "A Case of Canine Primitive Neuroectodermal Tumor (PNET)," *Journal of Veterinary Medical Science* 63, no. 1 (2001): 103–105, <https://doi.org/10.1292/jvms.63.103>.
6. J. Junginger, A. Röthlisberger, A. Lehmbecker, et al., "Peripheral Primitive Neuroectodermal Tumour in a Dog," *Journal of Comparative Pathology* 149, no. 4 (2013): 424–428.
7. L. Gao, Y. Zhu, X. Shi, et al., "Peripheral Primitive Neuroectodermal Tumors: A Retrospective Analysis of 89 Cases and Literature Review," *Oncology Letters* 18 (2019): 6885–6890, <https://doi.org/10.3892/ol.2019.11011>.
8. H. E. V. De Cock, M. D. M. Busch, M. M. Fry, et al., "A Peripheral Primitive Neuroectodermal Tumor With Generalized Bone Metastases in a Puppy," *Veterinary Pathology* 41, no. 4 (2004): 437–441.
9. S. Hosokawa, S. Suzuki, N. Hibino, et al., "Peripheral Primitive Neuroectodermal Tumor (Peripheral Neuroepithelioma) in a Dog," *Contemporary Topics in Laboratory Animal Science* 37, no. 1 (1998): 66–69.
10. P. Baillargeon, V. Fernandez-Vega, B. P. Sridharan, et al., "The Scripps Molecular Screening Center and Translational Research Institute," *SLAS Discovery* 24, no. 3 (2019): 386–397.
11. S. Hou, H. Tiriach, B. P. Sridharan, et al., "Advanced Development of Primary Pancreatic Organoid Tumor Models for High-Throughput Phenotypic Drug Screening," *SLAS Discovery* 23, no. 6 (2018): 574–584.
12. V. F. Vega, D. Yang, L. O. Jordán, et al., "Protocol for 3D Screening of Lung Cancer Spheroids Using Natural Products," *SLAS Discovery* 28, no. 2 (2023): 20–28.
13. M. J. Gains, M.-K. Leclerc, and C. Bédard, "A Primitive Neuroectodermal Tumor With Extension Into the Cranial Vault in a Dog," *Canadian Veterinary Journal* 52, no. 11 (2011): 1232–1236.
14. A. Keka-Sylaj, A. Ramosaj, A. Baloku, L. Zogaj, F. Mushica, and F. Kurshumliu, "Peripheral Primitive Neuroectodermal Tumor: A Case Report," *Journal of Medical Case Reports* 16, no. 1 (2022): 128.
15. J. M. Rafalko, K. M. Kruglyak, A. L. McCleary-Wheeler, et al., "Age at Cancer Diagnosis by Breed, Weight, Sex, and Cancer Type in a Cohort

of More Than 3,000 Dogs: Determining the Optimal Age to Initiate Cancer Screening in Canine Patients,” *PLoS One* 18, no. 2 (2023): e0280795.

16. G. Wang and F. Guo, “Primary Intramedullary Primitive Neuroectodermal Tumor: A Case Report and Review of the Literature,” *Medicine* 96, no. 49 (2017): e9001.

17. S. A. Headley, M. Koljonen, L. A. Gomes, and A. Sukura, “Central Primitive Neuroectodermal Tumour With Ependymal Differentiation in a Dog,” *Journal of Comparative Pathology* 140, no. 1 (2009): 80–83.

18. B. C. Mobley, D. Roulston, G. V. Shah, K. E. Bijwaard, and P. E. McKeever, “Peripheral Primitive Neuroectodermal Tumor/Ewing’s Sarcoma of the Craniospinal Vault: Case Reports and Review,” *Human Pathology* 37, no. 7 (2006): 845–853.

19. Z. Benbrahim, S. Arifi, K. Daoudi, et al., “Askin’s Tumor: A Case Report and Literature Review,” *World Journal of Surgical Oncology* 11, no. 1 (2013): 10.

20. K. Zhang, R. Lu, P. Zhang, et al., “Askin’s Tumor: 11 Cases and a Review of the Literature,” *Oncology Letters* 11, no. 1 (2016): 253–256.

21. S. Cao, X. Hu, S. Ren, et al., “The Biological Role and Immunotherapy of Gangliosides and GD3 Synthase in Cancers,” *Frontiers in Cell and Development Biology* 11 (2023): 1076862.

22. X. L. Pan, T. Izumi, H. Yamada, K. Akiyoshi, S. Suenobu, and S. Yokoyama, “Ganglioside Patterns in Neuroepithelial Tumors of Childhood,” *Brain and Development* 22, no. 3 (2000): 196–198.

23. E. Ulukaya, D. Karakas, and K. Dimas, “Tumor Chemosensitivity Assays Are Helpful for Personalized Cytotoxic Treatments in Cancer Patients,” *Medicina* 57, no. 6 (2021): 636.

24. F. Xia, S. Ma, Y. Bian, et al., “A Retrospective Study of the Correlation of In Vitro Chemosensitivity Using ATP-TCA With Patient Clinical Outcomes in Acute Myeloid Leukemia,” *Cancer Chemotherapy and Pharmacology* 85, no. 3 (2020): 509–515.

25. G. Kara Gedik, O. Sari, T. Altinok, L. Tavli, B. Kaya, and P. Ozcan Kara, “Askin’s Tumor in an Adult: Case Report and Findings on 18F-FDG PET/CT,” *Case Reports in Medicine* 2009 (2009): 1–4.

Supporting Information

Additional supporting information can be found online in the Supporting Information section.